



## A Revolutionary 5G-Based Real-Time Filtered-OFDM System for Off-Band Emission Reduction

Riyadh Kareem Jawad<sup>1</sup>, Ahmad Ghandour<sup>1</sup>, Mahmood Anees Ahmed<sup>2</sup>, Ahmad Taher Azar<sup>3,4,5</sup>,  
Syed Umar Amin<sup>3,4</sup>, Mohammed Abdul Majeed<sup>6</sup>, Zeeshan Haider<sup>3,4</sup>, Zafar Iqbal Khan<sup>3,4</sup>,  
Ibraheem Kasim Ibraheem<sup>6,7\*</sup>, Yousif I. Hammadi<sup>8</sup>

<sup>1</sup> Department of Computer Communication, College of Engineering, Islamic University of Lebanon, Beirut 2050, Lebanon

<sup>2</sup> Medical Instrumentation Techniques Engineering Department, College of Medical Techniques, Al-Farahidi University, Baghdad 10001, Iraq

<sup>3</sup> College of Computer and Information Sciences, Prince Sultan University, Riyadh 11586, Saudi Arabia

<sup>4</sup> Automated Systems and Soft Computing Lab (ASSCL), Prince Sultan University, Riyadh 11586, Saudi Arabia

<sup>5</sup> Faculty of Computers and Artificial Intelligence, Benha University, Benha 13518, Egypt

<sup>6</sup> Department of Cybersecurity and Cloud Computing, Technical Engineering, Uruk University, Baghdad 10001, Iraq

<sup>7</sup> Department of Electrical Engineering, College of Engineering, University of Baghdad, Baghdad 10001, Iraq

<sup>8</sup> Department of Medical Instrumentation Techniques Engineering, Bilad Alrafidain University College, Diyala 32001, Iraq

Corresponding Author Email: [ibraheemki@coeng.uobaghdad.edu.iq](mailto:ibraheemki@coeng.uobaghdad.edu.iq)

Copyright: ©2024 The authors. This article is published by IETA and is licensed under the CC BY 4.0 license (<http://creativecommons.org/licenses/by/4.0/>).

<https://doi.org/10.18280/mmep.111101>

### ABSTRACT

**Received:** 14 March 2024

**Revised:** 17 July 2024

**Accepted:** 24 July 2024

**Available online:** 29 November 2024

#### Keywords:

5G communication, F-OFDM, Windowed-Sinc filter design, Blackman-Harris window, Bohman window, BER, PSD, MATLAB simulation

In order to examine the 5G enhancement, this work generates a variety of Filtered-Orthogonal Frequency Division Multiplexing (F-OFDM) waveforms. Windowed-Sinc filters are studied to deploy waveforms in real time. The Blackman-Harris window and the Bohman window have been combined to create a new window, which has been studied. Waveforms built utilizing this window have been compared to traditional Cyclic Prefix Orthogonal Frequency Division Multiplexing (CP-OFDM) waveforms using the MATLAB evaluation package. Data from simulations reveals a number of tradeoffs between bit error rate (BER) and power spectral density. The designer, however, has some leeway in how the window is used. However, BER and power spectral density (PSD) measurements demonstrate that the windows chosen for this work nearly outperform the CP-OFDM signal. Compared to the central lobe, the sidelobe PSD of CP-OFDM is found to be close to -50dBW/Hz. However, -214.177 dBW/Hz is the value obtained for the new-window.

## 1. INTRODUCTION

High-speed Internet Protocol (IP)-based network of the third generation. The reason for the development of the 3G communication system was that cellular mobile phones became increasingly popular in daily life, particularly after the introduction of smartphones that support data communication applications; consequently, cell phones became an integral part of people's lives. In addition to the high data rate, the third generation supports multiple other services, including video calling and streaming, enhanced web perusing, and online gaming. As a result of the increased demand from subscribers and the industry community, it was necessary to develop a communication system capable of meeting all of these demands. Fourth Generation (4G) was the answer during the 3G era. 4G substantially increased the data rate, allowing simultaneous voice calls and data transmissions, thereby making high-definition streaming possible. Circuit switching is eliminated and substituted with packets, which is one of the primary benefits of 4G systems (all devices will have IP addresses).

Nevertheless, 4G was an improved version of 3G, dubbed 4G Long Term Evolution (LTE). The evolution of 4G LTE to 4G LTE-Advanced. In the past decade, new applications and industrial products have been introduced that necessitate a more advanced and rapid communication system due to technological advancements. Accordingly, Fifth Generation (5G) was proposed as an ultra-reliable system that offers a very rapid Internet connection, a greater number of connected devices in the unit area, and greater bandwidths. 5G used a variety of modulation formats to meet the requirements; these modulation formats are essentially asynchronous, allowing for greater flexibility in the communication link.

However, 5G is expected to deliver improved download/upload speeds compared to previous generations. Additionally, it should support various numerologies, such as sensors transmitting short messages. To achieve these objectives—delivering high speeds across different numerologies and ensuring service availability at any time— asynchronous communication is essential. The long tail of 4G pulses, which hinders asynchronous operations, must be eliminated. Various solutions have been proposed by both

industry professionals and academics, including online filter designs and other signal processing techniques, which will be discussed in the following section.

The goal is to minimize or eliminate out-of-band emissions (tails), thereby freeing up spectrum for both uplink and downlink transmissions. This approach will not only achieve higher throughputs across all numerologies but also liberate spectrum previously allocated to the synchronization process, resulting in faster connections to the station through noncoherent communication.

The definitions of technical terms are given below:

**F-OFDM:** A modulation scheme that uses filters to reduce out-of-band emissions, improving spectral efficiency.

**Windowed-Sinc filters:** A type of filter used in signal processing to smooth data and minimize noise.

**Blackman-Harris window and Bohman window:** Specific types of window functions used to design filters with particular characteristics.

**BER:** A measure of the number of bit errors in a transmission, indicating the reliability of the communication system.

**PSD:** A measure of the power present in a signal as a function of frequency.

The structure of this paper is as follows: Section 2 presents a literature review of the generations of F-OFDM implemented via various methods. Section 3 introduces the theoretical foundations of CP-OFDM and F-OFDM, followed by filter design suggestions for the F-OFDM waveform in Section 4. Section 5 discusses the simulations of both CP-OFDM and F-OFDM. The paper concludes with future work in Section 6.

## 2. PROBLEM STATEMENT: CHALLENGES AND LIMITATIONS OF EXISTING 5G WAVEFORMS

**Spectral efficiency:** Traditional 5G waveforms like OFDM have limitations in spectral efficiency, especially in scenarios with high spectral congestion. This inefficiency can lead to interference and reduced performance in densely populated areas.

**Interference management:** 5G networks often face significant challenges in managing inter-cell and intra-cell interference, which can degrade the overall quality of service.

**Latency:** Although 5G significantly reduces latency compared to previous generations, certain applications, such as ultra-reliable low-latency communications (URLLC), still require further enhancements to meet stringent latency requirements.

**Peak-to-Average Power Ratio (PAPR):** High PAPR in OFDM waveforms necessitates the use of linear power amplifiers, which are less power-efficient and can increase operational costs.

**Compatibility with Non-Orthogonal Multiple Access (NOMA):** Existing 5G waveforms may not be fully optimized for integration with advanced multiple access schemes like NOMA, which is crucial for enhancing user capacity and network efficiency.

## 3. RESEARCH GAPS AND OBJECTIVES

### 3.1 Research gaps

**Lack of enhanced spectral efficiency solutions:** Current

solutions do not sufficiently address the need for enhanced spectral efficiency in highly congested spectral environments.

**Insufficient interference management techniques:** There is a need for more robust interference management techniques that can be integrated seamlessly with existing 5G infrastructure.

**Inadequate low-latency solutions:** Existing waveforms fall short in meeting the ultra-low latency demands of emerging applications.

**PAPR reduction strategies:** Current approaches to reducing PAPR in OFDM are either too complex or not sufficiently effective.

**Integration with NOMA:** There is a gap in developing waveforms that are inherently compatible with NOMA, maximizing user capacity and efficiency.

### 3.2 Objectives of the work

**To develop a filtered-OFDM system:** Design and implement a Filtered-OFDM (F-OFDM) system that enhances spectral efficiency by minimizing out-of-band emissions and improving utilization of the available spectrum.

**To improve interference management:** Integrate advanced filtering techniques in the F-OFDM system to better manage inter-cell and intra-cell interference.

**To reduce latency:** Optimize the F-OFDM system to achieve lower latency, making it suitable for URLLC applications.

**To address PAPR issues:** Implement innovative techniques within the F-OFDM framework to reduce PAPR, improve power efficiency, and reduce operational costs.

**To ensure compatibility with NOMA:** Design the F-OFDM system to be compatible with NOMA, enhancing the overall capacity and efficiency of the 5G network.

## 4. LITERATURE REVIEW

In addition to the usual voice and data advantages of mobile phones, it is envisaged that the 5G system would support traffic that is generally distinct from the traditional ones, such as MTC, which utilizes extremely short messages, and the Internet of Things (IoT) [1]. Peak data rates, user-experienced throughput, cell average and edge spectral efficiency, control and user plane latency, dependability, connection density, efficiency, etc., were also agreed upon as performance measures. The 3GPP is still debating the precise values for the 5G KPIs.

In order to specify the physical layer elements of 5G, LTE, and the Universal Mobile Telecommunications System (UMTS)/high-speed packet access (HSPA) system, the actual work on the 5G channel model was transferred to 3GPP WG1 (workgroup number – 1) in January 2016. The three working group sessions held up until March 2016 saw significant progress, and a stochastic model was selected as the required model and a hybrid model as the optional model. The technical paper for channel modeling included both models [2]. The majority of the requirements [3] work at the RAN level was completed by March 2016. The eMBB, URLLC, and mMTC deployment scenarios were determined to be the three most crucial ones for the requirements.

The 3GPP approved a study item in March 2016 to look at various technologies for 5G new radio (NR) [4]. The name "new radio" was chosen since no 4G standard, including LTE

Advanced Pro, will be backward compatible with this air interface. This novel radio interface can be used as a stand-alone network, meaning it is independent of existing networks. The time-domain localization characteristic in 5G waveforms is also needed to enable the necessary latency and short message delivery despite the asynchronization of transmission [5]. Filtered signals have, therefore, been widely discussed recently in order to certify the waveform of the 5G networks. This means that recommended filter-based waveforms outperform OFDM since they can enable asynchronous transmission while reducing out-of-band (OOB) emission [6]. Subcarrier-based filtering, subband-based filtering, and whole band-based filtering are the three categories into which these filtered waveforms can be divided. Filterbank Multicarrier (FBMC) [7] beats traditional CP-OFDM, which employs offset QAM (OQAM) [8, 9]. Generalized Frequency Division Multiplexing (GFDM) [10, 11] is another subcarrier filtering-based waveform. The extended tail of the filter impulse response, despite the strong features produced, decreases latency, a crucial attribute in 5G systems [12]. One of the stated remedies for the long tail was offered by Bellanger et al. [7], although the latency was increased. The loss of complex orthogonality, which results in inter-symbol interference, is another drawback of FBMC [13-15].

The second kind, subband-based filtered waveforms, was created to address the problems mentioned earlier. This method will set up the filter to cover a subband where many subcarriers are available for transmission. In other words, because of the greater filter bandwidth, the filter's impulse response will be shorter than in the case of per subcarrier filter operation. The resource block filtered OFDM was established because each subband in LTE designs consists of 12 subcarriers, which is referred to as an RB [16]. The universal filtered multicarrier (UFMC), which falls under the subband-based filtering group, was another recommended choice for 5G [13]. Just one filter is required per subband at the transmitter when UFMC filtering is only performed on the transmitter side. The filter bandwidth can be raised further so that the whole transmitted subband bandwidth will be simultaneously filtered. In other words, the transmitter will only use one filter. Filtered-OFDM (F-OFDM) is the name given to this type of filtered signal [17, 18]. It is important to note that FBMC and F-OFDM are both special instances of UFMC. By lowering the filter size to one subcarrier width, UFMC becomes FBMC, and by raising the filter width to the entire allotted bandwidth, UFMC becomes F-OFDM, thus the term Universal Filtered Multicarrier.

To reduce synchronization requirements, various waveforms have been proposed, with OOB emission avoidance being a primary motivation for asynchronous transmission [15, 19, 20]. Abdoli et al. [18] recommend eliminating the lengthy tail impulse response of conventional CP-OFDM and suggest using F-OFDM in an asynchronous multi-user system. Although UFMC may support the same features as F-OFDM, F-OFDM is considered more effective [17, 18, 21]. Using a similar approach conducted by Abdoli et al. [18] but employing the Von Hann window, Bazzi et al. [22] developed a filter that significantly outperforms both FBMC and UFMC. Further insights into F-OFDM are provided by Wu et al. [23], where a real-world field test demonstrated its superior performance compared to CP-OFDM. Additionally, Hu and Armada [24] showcased F-OFDM's capability to manage heterogeneous numerologies through their analysis of MTC and conventional voice transmissions.

Augustine et al. [25] have designed a Hanning-based filter according to the finite impulse response filters technique. They showed that the minimum stopband they reached was around -100dB with respect to the main lobe. The total number of taps used in the filter was 128, according to the finite impulse response design. A comparative study of various modulation types for the 5G applications was reported by Ramineni et al. [26]. The study evaluation parameters are power spectral density, bit error rate, and out-of-band emission. It was found that UFMC and F-OFDM signals have reduced out-of-band emission, but if compared to FBMC, the FBMC shows a significant improvement in the out-of-band suppression. However, the authors did not mention the filter type that they have employed in their investigation. Others proposed continuous phase modulation (CPM) in order to mitigate different limitations in the 5G communication systems [27]. However, CPM produced has its limitations, specifically the limited download speeds.

The next section will show the main concepts of 5G and other previous generations, such as CP-OFDM, which stands for the 4G systems. Furthermore, the connection between the conventional OFDM and the F-OFDM will be introduced.

## 5. THEORETICAL BACKGROUND

### 5.1 5G air interface

The numerologies ( $\alpha$ ), which range from sub-6 GHz to mm-waves, are the most important parts of the 5G air interface. In other words, the formula [28] says that the distance between subcarriers can be anywhere from 15 KHz to 240 KHz.

$$\Delta f = 2^\alpha \times 15 \text{ KHz} \quad (1)$$

where,  $\alpha$  is equal to 0, 1, 2, 3, or 4, the first three scales,  $\alpha = 0, 1, \text{ and } 2$ , are for large cells that work below 6 GHz with normal CP, except for 60 KHz, which works with both normal and extended CP. While other scales are for small cells and work with frequencies higher than 6 GHz and normal CP durations. So, the frame structure, which still has a  $T_f=10\text{ms}$  length, can now support different numbers [28, 29],

$$T_f = \frac{\Delta f_{max} N_f}{100} \times T_c \quad (2)$$

where,  $N_f$  is constant equal to 4096,  $\Delta f_{max} = 480\text{KHz}$ , and  $T_c = 1/(\Delta f_{max} N_f)$  [28, 30, 31]. Each frame is split into ten subframes, and each one lasts 1 ms, just like LTE. Based on the subcarrier spacing,  $\Delta f$ , and the fact that each subframe has a different number of slots, each subframe takes up 14 OFDM symbols. In the third row, 14 stands for normal, and 12 stands for extended. Still, any slot can send in either the downlink or the uplink direction or in both directions. Also, the data being sent cannot take up an entire slot. RBs are groups of REs. Each RB has 12 subcarriers. This is similar to how LTE is set up.

### 5.2 CP-OFDM model

Multiplexing using cyclic prefix orthogonal frequency division is a subset of multicarrier modulation methods. In the first step, binary data are mapped to a constellation diagram [32, 33]. There are three possible constellation orders: QPSK (Quadrature Phase Shift Keying), 16-Quadrature Amplitude

Modulation (16-QAM), and 64-QAM. The system implemented one of these orders based on the required data throughput, cell size, and channel quality indicator. After data mapping, serial to parallel demultiplexing occurs. In other words, serial frequency-domain data are translated to parallel form. The optimum implementation of the Inverse Discrete Fourier Transform (IDFT) block is the fast variant (Inverse Fast Fourier Transform) IFFT at this point. The IFFT block will convert frequency-domain data to time-domain data. For flexible bandwidth allocations, Inverse/Fast Fourier Transform (IFFT) may be scaled from 128 to 2048 points in size.

Extended or regular CP will be blended with the signal following frequency-to-time domain conversion. The purpose of CP insertion is to join the message vector's tail to its head. The signal is then prepared for multiplexing, or, to put it another way, it will be changed from parallel to serial format so that it may be transferred to the channel. The signal will have Additive White Gaussian Noise (AWGN) added to it as the propagation channel.

The signal travels through the opposite processes of the transmitter at the receiving end. The signal will first be demultiplexed or changed from serial to parallel form after being received. After the demultiplexing, the CP that was added at the transmitter to get rid of ISI and maintain orthogonality during channel propagation would be taken away at the receiver. The signal will next be passed to the FFT

$$\mathbf{W} = \frac{1}{\sqrt{N_{fft}}} \begin{bmatrix} w^{-0 \times 0} & w^{-0 \times 1} & \dots & w^{-0 \times (N_{fft}-1)} \\ w^{-1 \times 0} & w^{-1} & \dots & w^{-(N_{fft}-1)} \\ w^{-2 \times 0} & w^{-2} & \dots & w^{-2(N_{fft}-1)} \\ \vdots & \vdots & \ddots & \vdots \\ w^{-(N_{fft}-1) \times 0} & w^{-(N_{fft}-1)} & \dots & w^{-(N_{fft}-1)(N_{fft}-1)} \end{bmatrix} \quad (5)$$

in which,  $w$  is the twiddle factor that can be determined as,

$$w = e^{\frac{j2\pi}{N_{fft}}} \quad (6)$$

Accordingly, Eq. (3) can be reformulated in a matrix form as follows,

$$= \frac{1}{\sqrt{N_{fft}}} \begin{bmatrix} 1 & 1 & \dots & 1 \\ 1 & w^{-1} & \dots & w^{-(N_{fft}-1)} \\ \vdots & \vdots & \ddots & \vdots \\ 1 & w^{-(N_{fft}-1)} & \dots & w^{-(N_{fft}-1)(N_{fft}-1)} \end{bmatrix} \begin{bmatrix} x(0) \\ x(1) \\ \vdots \\ x(N_{fft}-1) \end{bmatrix} \quad (7)$$

$$\times \begin{bmatrix} X(0) \\ X(1) \\ \vdots \\ X(N_{fft}-1) \end{bmatrix}$$

Consequently, after the CP part is included, the signal will travel the whole channel. After removing the CP portion from the receiver,

$$\hat{\mathbf{X}} = \mathbf{W}^{-1} \times \mathbf{W} \times \mathbf{X} \quad (8)$$

where,  $x$  is the constellation point that was obtained following the DFT operations in the previous equation. These are all the

block, a time-to-frequency-domain converter. Via the multiplexer, serialize the FFT block's output. Finding the signal in the last block will now include decoding the discrete signal into binary data, which will then serve to represent the signal that was received.

The equation of IDFT pair may best be used to express the mathematical form. The IDFT and the receiving end by the DFT represent the transmitting end.

$$x(n) = \frac{1}{\sqrt{N_{fft}}} \sum_{k=0}^{N_{fft}-1} X(k) e^{j2\pi \frac{kn}{N_{fft}}} \quad (3)$$

where,  $n, k = 0, 1 \dots N_{fft} - 1$  are time and frequency indices, respectively,  $N_{fft}$  stands for the number of subcarriers in one OFDM symbol,  $X(k)$  represents the constellation points, which are either QPSK, 16-QAM, or 64-QAM levels according to the required throughput and channel impairments. These constellation points represent the binary input data to the system. In compact form, the OFDM signal,  $x(n)$  can be written in matrix format as,

$$\mathbf{x} = \mathbf{W} \times \mathbf{X} \quad (4)$$

where,  $\mathbf{X}$  is the input integer data vector to the IFFT block, and  $\mathbf{W}$  is an  $N_{fft} \times N_{fft}$  square transformation matrix.

procedures that take place throughout the signal's trip through the CP-OFDM system. The alternative potential signal travel in the 5G system is shown in the next section.

The block diagram structure of the filtered-OFDM resembles that of CP-OFDM. The upper portion will be repeated in accordance with the available bandwidth, but depending on the use case, each repetition will utilize a different size of  $N_{fft}$  and a different subcarrier spacing,  $\Delta f$ .

Figure 1 illustrates multiple numerologies of F-OFDM block diagrams, while Figure 2 details the receiving process.

To begin with, various numerology instances require various subcarrier spacings. Figure 1 clearly illustrates this. A mapping operation is implemented, followed by demultiplexing, and then an IFFT operation with various sizes, depending on the particular case. To ensure that the signal is precisely CP-OFDM, demultiplexing and CP insertion must be performed. The filter will be applied after the CP-OFDM generation in F-OFDM, which is a distinction. The results signal, as previously discussed in this section, has features different from those of CP-OFDM.

The receiver, on the other hand, must recover every sub-band to its intended location. The transmitter operates in reverse, and this is done. As shown in Figure 2, the signal will first undergo filter-free effect (removing the transmitter side's filter effect), followed by CP removal, serial to parallel conversion, and FFT operation with corresponding  $N_{fft}$  for each sub-band. Finally, the signal will be re-multiplexed to be detected by the de-mapping block.

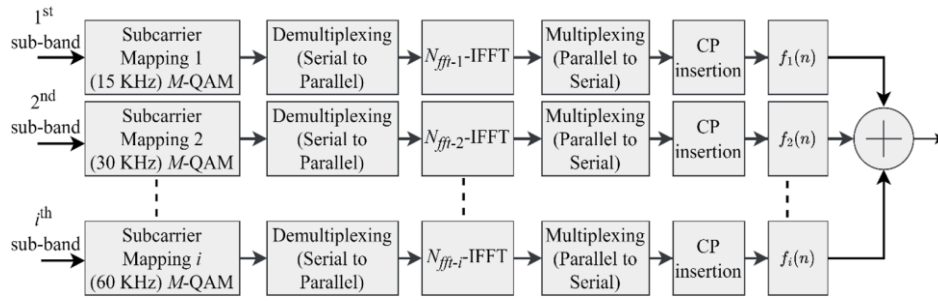


**Figure 1.** The F-OFDM block diagram shows different numerologies on the transmitter system side

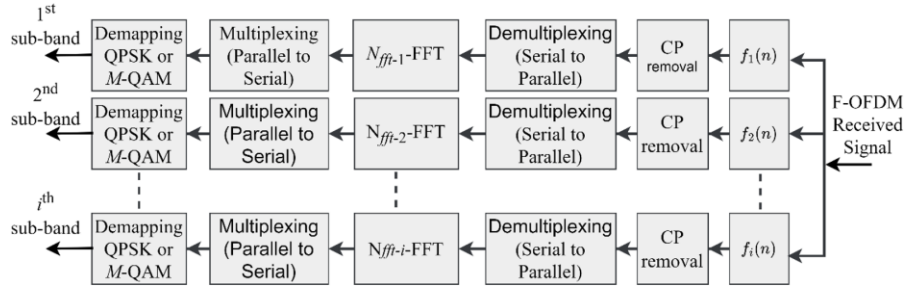


**Figure 2.** F-OFDM block diagram showing different numerologies on the receiving system side

By mixing several numerologies, such as  $i = 1, 2 \dots I$ , where  $I$  is the total number of numerologies utilized in the transmitted signal, one may mathematically define F-OFDM as a combination of these numerologies as,

$$\check{x}(n) = \sum_{i=1}^I \frac{1}{\sqrt{N_{fft-i}}} \sum_{k=0}^{N_{fft-i}-1} X_i(k) e^{j2\pi \frac{kn}{N_{fft-i}}} \quad (9)$$

In other words, several  $I$  numerologies make up the signal

$$\check{x}_f(n) = \left[ \sum_{i=1}^I \frac{1}{\sqrt{N_{fft-i}}} \cdot \sum_{m=-\infty}^{\infty} f_i(n-m) \sum_{k=0}^{N_{fft-i}-1} X_i(k) e^{j2\pi \frac{km}{N_{fft-i}}} \right] \quad (10)$$

where,

$\check{x}_f(n)$  is the time-domain representation of the filtered OFDM signal.

$X_i(k)$  is the frequency-domain representation of the OFDM signal for the  $i$ -th subband.

$f_i(n)$  is the filter applied to the  $i$ -th subband.

$N_{fft-i}$  is the size of the FFT for the  $i$ -th subband.

This equation highlights the convolution of the OFDM signal with the filter in the time domain, demonstrating the filtering effect on the subband signals. The filtering process reduces out-of-band emissions and ensures efficient spectral

$$W_i = \frac{1}{\sqrt{N_{fft-i}}} \begin{bmatrix} w_i^{-0 \times 0} & & w_i^{-0 \times 1} & & w_i^{-0 \times 2} & \dots & w_i^{-0 \times (N_{fft-i}-1)} \\ w_i^{-1 \times 0} & & w_i^{-1} & & w_i^{-2} & \dots & w_i^{-(N_{fft-i}-1)} \\ w_i^{-2 \times 0} & & w_i^{-2} & & w_i^{-4} & \dots & w_i^{-2(N_{fft-i}-1)} \\ \vdots & & \vdots & & \vdots & \ddots & \vdots \\ w_i^{-(N_{fft-i}-1) \times 0} & & w_i^{-N_{fft-i}-1} & & w_i^{-2(N_{fft-i}-1)} & \dots & w_i^{-(N_{fft-i}-1)(N_{fft-i}-1)} \end{bmatrix} \quad (12)$$

The block diagram of the transmitting-sided F-OFDM system depicted in Figure 1 is now represented by Eq. (13). The first step at the receiver is to eliminate the filter effect by deconvolving the numerologies of the signal with the

$\check{x}$ . Hence, Eq. (9) stands for a specific numerology, a single branch, which is indeed one branch of CP-OFDM. Each CP-OFDM symbol has a numerology that is identical to a specific branch in Figure 1. Because of this, F-OFDM has a wide range of numerologies. Unfortunately, the signal  $\check{x}$  is not filtered up to this level; therefore, before it is filtered for F-OFDM,  $\check{x}$  should be filtered. Thus, each filter will correspond to a branch in Figure 1. Therefore, Eq. (11) shows a summation of various branches that represent different numerologies.

utilization.

The filter used in the final equation,  $f_i(n)$ , will be covered in the following section. As the CP-OFDM matrix format representation is transferable to F-OFDM,

$$\check{x}_f = [W_i \times X_i] \cdot F_i \quad (11)$$

Since  $F_i$  is the frequency domain of the  $f_i$  filter, and depending on the use case, the transformation matrix now has varying dimensions, where the twiddle factor remained unchanged, Eq. (11) can thus be rewritten as follows:

corresponding filters; in other words, the signal is passed through the filter  $f_i^*(-n)$ , which is matched to the filter at the transmitter.

$$\begin{bmatrix} \check{x}_f(0) \\ \check{x}_f(1) \\ \vdots \\ \check{x}_f(N_{fft-i}-1) \end{bmatrix} = \frac{1}{\sqrt{N_{fft-i}}} \begin{bmatrix} 1 & 1 & \dots & 1 \\ 1 & w_i^{-1} & \dots & w_i^{-(N_{fft-i}-1)} \\ \vdots & \vdots & \ddots & \vdots \\ 1 & w_i^{-(N_{fft-i}-1)} & \dots & w_i^{-(N_{fft-i}-1)(N_{fft-i}-1)} \end{bmatrix} \times \begin{bmatrix} X_i(0) \\ X_i(1) \\ \vdots \\ X_i(N_{fft-i}-1) \end{bmatrix} \cdot \begin{bmatrix} F_i(0) \\ F_i(1) \\ \vdots \\ F_i(N_{fft-i}-1) \end{bmatrix} \quad (13)$$

$$\check{x}_f^r(i, n) = \check{\mathbf{X}}_f * f_i^*(-n) \quad (14)$$

$$\check{x}_f^r(i, n) = \frac{1}{\sqrt{N_{fft-i}}} \sum_{m=-\infty}^{\infty} f_i^*(n-m) \sum_{k=0}^{N_{fft-i}-1} X_i(k) e^{j2\pi \frac{km}{N_{fft-i}}} \quad (15)$$

Next, as shown in Figure 2, the signal is prepared for CP removal, demultiplexing, and time-to-frequency conversion using the appropriate FFT, multiplexing, and detection (demapping). The F-OFDM signal's trip concludes this stage when the signal is retrieved according to Eq. (15). To determine the quality of the received signal, though, it must first be assessed. BER and PSD will be briefly reviewed in the sections that follow.

On the other hand, one of the performance evaluation techniques used in this thesis is PSD. Before it is used in the next sections, it must first be explained. There are several methods for estimating the PSD. The periodogram PSD estimate technique will be used in this thesis [34]. One non-parametric estimating technique is the periodogram approach.

$$PSD = \frac{1}{Nf_s} \left| \sum_{n=0}^{N-1} x(n) e^{-j2\pi f n} \right|^2 \quad (16)$$

where,  $-f_s/2 < f \leq f_s/2$  and  $f_s$  is the sampling frequency.  $x(n)$  is the time-domain signal. As a result, the time-domain signal's discrete DFT is all that the spectral estimate is. But if a window function is added to the time-series signal,  $x(n)$ , the outcome is the so-called modified periodogram spectral estimating technique. The window function that may decay to zero at both ends and is not negative was chosen. Hence, the updated periodogram PSD method is

$$PSD = \frac{1}{Nf_s} \left| \sum_{n=0}^{N-1} [x(n) \cdot s(n)] e^{-j2\pi f n} \right|^2 \quad (17)$$

where,  $s(n)$  is the window function. The PSD performance of the proposed F-OFDM will be assessed using the modified periodogram approach described in the previous formulation in order to compare it to the traditional CP-OFDM, which will also be calculated using the modified periodogram technique in the next sections of this paper.

## 6. PROPOSED METHODOLOGY

### 6.1 Filter design approach

Several types of interchanging windows, which are made up of two or sometimes more windows, have been suggested by previous research. The target was a window with significantly less sidelobe compared to what was used as a baseline. Bartlett window is created by convolving two rectangular windows. Hamming window is created by adding a Hanning window to a rectangular window, and the de la Valle-Poussin window is created by convolving two triangular windows of half-extent

[34].

It is also possible to create a new window, the cosine-tapered window, or Tukey window, by multiplying a rectangular window in the frequency domain by the cosine lobe or by convolution of the cosine lobe with the rectangular window in the time domain. Bohman window can be realized by convolving together two cosine lobe (or half-duration) windows; in other words, Bohman window is the time domain product of a triangular window and a cosine cycle. Imagine the well-known Hanning-Poisson window, which is the product of the Hanning window and the Poisson window [35].

The performance of F-OFDM, as mentioned earlier, is heavily dependent on the design of the filters in order to achieve finer time and frequency adaptation and increase the efficiency of the spectrum. The Windowed-Sinc method is an easy-to-implement online technique that is practical in software-defined radio (SDR) and is simple and systematic. Keep in mind that the primary objective of using a filter is to achieve an appropriate attenuation at the stopband such that interference with neighboring subcarriers is negligible; this allows the filter to handle interference from other nearby spectrums, meaning that it is feasible to coexist with older generations, such as 2G, 3G, and 4G [36-44].

Taher et al. [36] showed the generation of different Windowed-Sinc filters. According to what has been stated above, this section will follow the tradition of the literature and perform a convolution (multiplication in time-domain) between two time-domain windows,  $w_1(n)$  and  $w_2(n)$ .

$$w_3 = w_1(n) \cdot w_2(n) \quad (18)$$

Window functions are used in signal processing to mitigate the effects of spectral leakage by shaping the time-domain signal before it undergoes a Fourier transform. Common window functions include the Blackman-Harris and Bohman windows, each with distinct properties in terms of main lobe width and sidelobe suppression. The Blackman-Harris window is known for its excellent sidelobe suppression, making it ideal for minimizing interference from adjacent frequency bands. However, it has a relatively wide main lobe, which can reduce frequency resolution. The Bohman window, on the other hand, offers a narrower main lobe, providing better frequency resolution but with slightly higher sidelobes compared to Blackman-Harris.

By combining these two windows, we aim to achieve a balance between the main lobe width and sidelobe suppression, optimizing both frequency resolution and interference mitigation. The process of combining the Blackman-Harris and Bohman windows involves creating a hybrid window function that incorporates the advantages of both.

Another way of putting it is to think of  $w_3(n)$  as the output of the process recognized as windowing the first window,  $w_1(n)$ , by the second window,  $w_2(n)$ , or vice versa. In this work, it is suggested that the Bohman window is the Blackman-Harris window [35]. In other words,  $w_1(n)$  will be Blackman-Harris window and  $w_2(n)$  is the Bohman window,

$$w_1(n) = c_0 - c_1 \cos\left(\frac{2\pi n}{L-1}\right) + c_2 \cos\left(\frac{4\pi n}{L-1}\right) - c_3 \cos\left(\frac{6\pi n}{L-1}\right) \quad (19)$$

where,  $0 \leq n \leq L-1$  and  $L$  stands for the total length of the window. Moreover,  $c_0, c_1, c_2, c_3,$  and  $c_4$  are 0.35875, 0.48829, 0.14128, and 0.01168, respectively. While Bohman window is expressed as,

$$w_2(n) = (1 - |z|) \cos(\pi|z|) + \frac{1}{\pi} \sin(\pi|z|) \quad (20)$$

where,  $z$  is a normalized vector between -1 and +1 of length  $L$ , and the first and last values of this vector are equal to zero (forced), worthy mentions that this window, Bohman, is the result of the frequency-domain-convolution of two cosine lobes (of half-duration). In the time-domain, it was produced by the multiplication of triangular and cosine (single-cycle) windows and a term added in order to set the boundaries to zero (by setting the first derivative to zero) [35]. Accordingly, the new window will be,

$$w_3(n) = c_0 w_2(n) - c_1 w_2(n) \cos\left(\frac{2\pi n}{L-1}\right) + c_2 w_2(n) \cos\left(\frac{4\pi n}{L-1}\right) - c_3 w_2(n) \cos\left(\frac{6\pi n}{L-1}\right) \quad (21)$$

The last expression is representing the frequency domain of the new window,  $w_3(n)$ , which will be utilized as a window of view in this work. Hence, the new window will be used to truncate the sinc-function. However, let us understand it another way. It is assumed that the required filter response in the time domain is  $f_r(n)$ ,

$$f_r(n) = \frac{1}{2\pi} \int_{-\omega_c}^{\omega_c} e^{j\omega n} d\omega = \frac{\sin(\omega_c n)}{\omega_c n} \quad (22)$$

where,  $\omega_c$  is the cut-off frequency. The combined window function used in this study is a product of these two windows, ensuring the benefits of both are retained. The Sinc-function will be windowed using  $w_3(n)$ ,

$$f_{new}(n) = f_r(n) \cdot w_3(n) \quad (23)$$

Note that the last expression is a time-domain processing. Or it can be formulated as, using Eq. (21),

$$f_{new}(n) = \frac{\sin(\omega_c n)}{\omega_c n} \cdot w_3(n) \quad (24)$$

The proposed hybrid window combining the Blackman-Harris and Bohman windows offers several advantages over using each window individually:

**Enhanced sidelobe suppression:** The hybrid window maintains the excellent sidelobe suppression characteristic of the Blackman-Harris window, reducing interference from adjacent frequency bands.

**Improved frequency resolution:** By incorporating the narrower main lobe of the Bohman window, the hybrid window achieves better frequency resolution, allowing for more precise signal analysis.

**Flexibility:** The weighting factor  $\alpha$  provides flexibility in

tuning the hybrid window for specific applications, making it adaptable to various signal processing requirements.

The F-OFDM signal will be programmed using MATLAB to be simulated in the next section, according to the derived filter in this section. Hence, the F-OFDM signal can be formulated as,

$$\check{x}_f(n) = \left[ \frac{1}{\sqrt{N_{fft}}} \sum_{m=-\infty}^{\infty} f_{new}(n-m) \sum_{k=0}^{N_{fft}-1} X(k) e^{j2\pi \frac{km}{N_{fft}}} \right] \quad (25)$$

where, these last formulae will be used in the next section.

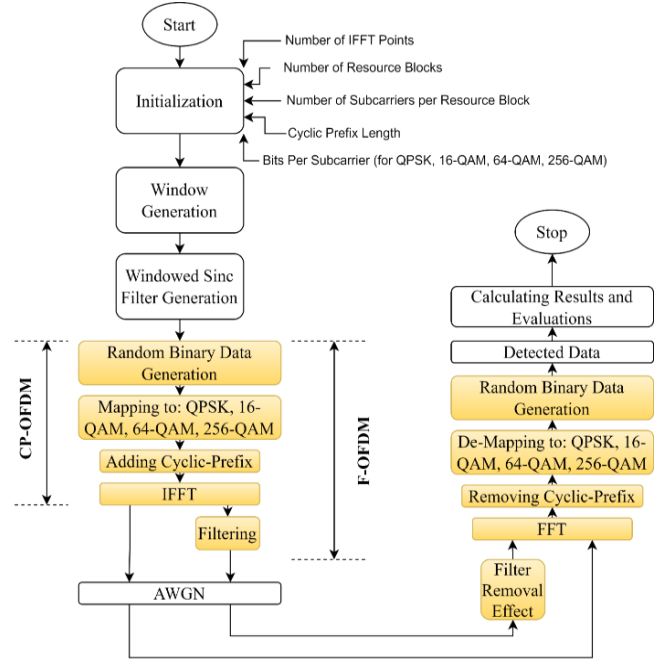


Figure 3. CP/F-OFDM systems simulation flow-chart

## 6.2 Methodology simulation flow

The primary objective of our filter design is to enhance the spectral efficiency of the F-OFDM system by minimizing out-of-band emissions. In our approach, we employ Windowed-Sinc filters in our F-OFDM system. The Windowed-Sinc filter is designed by multiplying the Sinc function with a window function to control the sidelobe levels. The designed filters are applied to the OFDM subcarriers to generate the F-OFDM signal. MATLAB R2021a functions are used to implement these filters and apply them to the OFDM symbols; Communications System Toolbox for OFDM and F-OFDM signal generation and analysis are used in these experiments. Figure 3 depicts the F-OFDM system's simulation flowchart. It is demonstrated that the first step is the system initialization, where the simulation scenarios will select the values for the CP length, the bits per subcarrier, the number of FFT points, the number of resource blocks, and the number of subcarriers inside a resource block. Second, windows must be created. The Windowed-Sinc are then determined. Hence, QPSK, 16-QAM, 64-QAM, and 256-QAM random binary data will be created and mapped in the next phase according to the constellation order. CP insertion and the IFFT procedure yield CP-OFDM, and the application of the Windowed-Sinc filter yields F-OFDM. However, the mapping operation is where the two signals are mostly formed. The AWGN channel was employed in this study. F-OFDM will have its filter impact

eliminated after the AWGN channel, while CP-OFDM will be transmitted directly into the FFT process. So, the CP will be eliminated, and the signal will be prepared for the de-mapping process, which will allow the transmitted data to be recovered. This stage allows for the computation of evaluation parameters that can then be recorded/plotted for later comparisons and comments.

## 7. RESULTS AND DISCUSSION

In this section, the suggested F-OFDM system will be simulated using MATLAB along with the CP-OFDM system. In other words, the system shown in Figure 3 will be implemented using MATLAB. This section will focus on establishing the required parameters for operating F-OFDM and CP-OFDM. Because of this, the simulation will be run with these specifications. Fifth-generation (5G) signals, represented by the F-OFDM waveform, and fourth-generation (4G) signals, represented by the CP-OFDM signal, will be modeled using evaluation techniques such as PSD and BER.

### 7.1 Simulation parameters settings

In this subsection, it is assumed that the bandwidth is 1.4MHz. If  $N_{FFT}=128$  subcarriers, then the OFDM size is 128. The number of subcarriers should dictate the length of the filter. In order to achieve a better harmony between time and frequency localizations, the literature has demonstrated that the filter length of F-OFDM can be more than the CP length. On a comparable basis, filter length will be determined in accordance with CP-OFDM requirements, nevertheless. Thus, one can determine the filter length ( $L$ ) by,

$$L = \frac{N_{FFT}}{2} - 1 \quad (26)$$

According to Eq. (26), the filter length, in this case, is 63 points. The load requirement determines how big a map of the constellations may be. Yet, in the present circumstance, all proposed constellation orders will be used, including QPSK, 16-QAM, 64-QAM, and 256-QAM schemes. Each of the six RBs will have 12 subcarriers for a total of 1.4 MHz. The 15 kilohertz between subcarriers is a hard limit. Finally, the ramp-up and ramp-down transition phases, both of which are part of the total transition time, are limited to 2.5 subcarriers [15]. Table 1 details the configuration settings in question.

**Table 1.** List of simulation parameter settings

Parameter	Value Set
NFFT	128
Length of cyclic prefix	72
Length of the proposed filter	63
Constellation mapping	QPSK, 16-QAM, 64-QAM, 256-QAM
Total number of RBs	6
Total number of subcarriers per RB	12
Ramp up/downsize	2.5-subcarriers
Subcarrier spacing (in KHz)	15
Channel	AWGN
SNR ranges	For QPSK: -20dB to 10dB Others: -10dB to 10dB

## 7.2 Simulation results and discussion

In this section, the simulation results based on the parameters set in the previous session will be discussed. First, the shape of the suggested window in the time domain will be compared with other standard windows. Second, the frequency domain of the suggested window will be discussed. Third, the power spectral density (PSD) of the F-OFDM signal will be shown based on the standard and proposed windows. Finally, the BER of the resultant F-OFDM signals will be discussed.

### 7.2.1 Time-domain windows

Figure 4 displays four time-domain windows: Exact Hamming, Minimum 4-terms Blackman Harris window, Bohman window, and the suggested window,  $W_3$ . It shows that the widest window is the Exact Hamming, while the narrowest window is the suggested window,  $W_3$ . The Minimum 4-terms Blackman Harris window and Bohman window fall between the Exact Hamming and the suggested window in terms of width. In other words, the suggested window is the best among the others. That is, this is the first indication that the proposed window has significant behavior in reducing the OOB emission if it is utilized to build the F-OFDM signal.

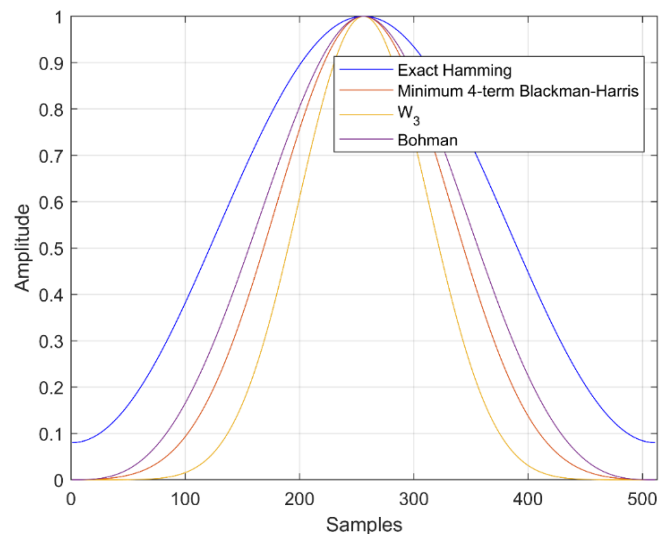


**Figure 4.** Time-domain comparison between the suggested window ( $W_3$ ), minimum 4-term Blackman-Harris window, Bohman window, and the Exact Hamming window

### 7.2.2 Frequency-domain windows

The frequency domain of the window itself (not employed yet to create the F-OFDM signal) can be seen in Figure 5. Thus, there are four windows in Figure 5, the same windows in Figure 4, but here they are in the frequency domain. It can be seen that the suggested window is superior to the others in terms of the first sidelobe value. In this scenario, the proposed window achieved -105.299 dBW/Hz, while the other windows are higher. For instance, Exact Hamming, Minimum 4-terms Blackman Harris window, and Bohman window are -61.6 dBW/Hz, -104.3 dBW/Hz, and -61.63 dBW/Hz, respectively. Accordingly, the proposed window,  $W_3$ , has a dramatic improvement with respect to the other windows, which is the second indication that  $W_3$  will be the proper window to be used for the F-OFDM signal. Thus, the OBE will be reduced if this  $W_3$  window is employed to generate the F-OFDM signal, as will be shown later in the next subsection.

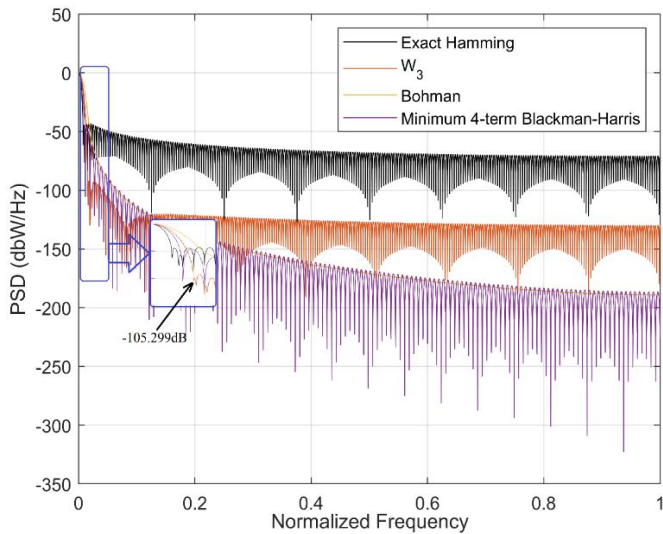


**Figure 5.** Frequency-domain comparison between the suggested window ( $W_3$ ), minimum 4-term Blackman-Harris window, Bohman window, and the Exact Hamming window

The combined window exhibits lower side lobe levels compared to traditional CP-OFDM windows, as evidenced by the  $-214.177$  dBW/Hz sidelobe power spectral density compared to CP-OFDM's  $-50$  dBW/Hz.

### 7.2.3 F-OFDM PSD

It has been seen that the proposed window has a superior performance both in the time and frequency domains, as indicated in Figure 4 for the time domain and Figure 5 for the frequency domain. Thus, it is time to utilize it in the generation process of the F-OFDM signal. Figure 6 shows the PSD of the CP-OFDM, which is the reference or the benchmark for this work, compared with the generated F-OFDM based on the  $W_3$ -window (the suggested window), minimum 4-term Blackman-Harris window, Bohman window, and the Exact Hamming window. It can be recognized that  $W_3$ -window outperforms the other windows-based F-OFDM signal as well as the CP-OFDM signal.

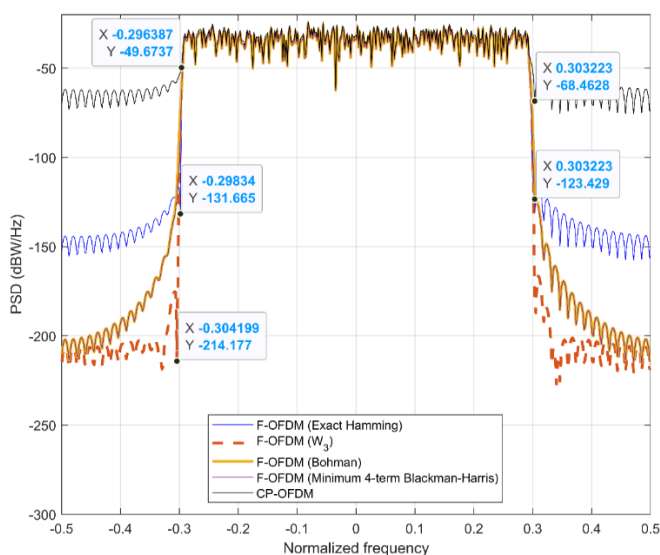


**Figure 6.** PSD comparison of the F-OFDM based on the suggested window ( $W_3$ ), minimum 4-term Blackman-Harris window, Bohman window, Exact Hamming window, and the conventional CP-OFDM signals

That is, CP-OFDM, as a reference, achieved  $-49.67$  dBW/Hz. F-OFDM-based Exact Hamming window improved the PSD to  $-131.665$  dBW/Hz. Further, the F-OFDM-based Bohman window reached  $-123.429$  dBW/Hz, and the F-OFDM-based minimum 4-term Blackman-Harris window achieved PSD of  $-68.4628$  dBW/Hz. On the other hand, the F-OFDM-based  $W_3$ -window has achieved the lowest PSD,  $-214.177$  dBW/Hz, which is the most significant improved value with respect to other windows-based F-OFDM and the bench-march (CP-OFDM) signals. Thus, it is indicated previously in Figure 4 and Figure 5 that the suggested window will be superior among others, and here in Figure 6, the results are true. The suggested Windowed-Sinc filter in this work has shown an improved result when compared with other works in the literature. For instance, the findings of Zhang et al. [17] suggest that the best stopband achieved was around  $-80.0$  dBW/Hz, and as reported by Abdoli et al. [18], the achieved stopband was around  $-100.0$  dBW/Hz.

### 7.2.4 F-OFDM BER results

The BER will be presented in this subsection for the QPSK, 16-QAM, 64QAM, and 256QAM-based F-OFDM signals. In Figure 7, the BER for each of the F-OFDM based on Minimum 4-term Blackman-Harris, Bohman, Exact Hamming, and the  $W_3$  windows almost have the same behavior, where the BER stops at SNR of 8 dB, just like the CP-OFDM. Since the QPSK mapping needs low power (SNR), the plot starts at  $-20$  dB in steps of 2 dB up to 10 dB. Thus, the suggested F-OFDM, which is based on the new window,  $W_3$ , did not diverge or degrade. Hence, the suggested window is sufficient for the F-OFDM to reduce the OBE.

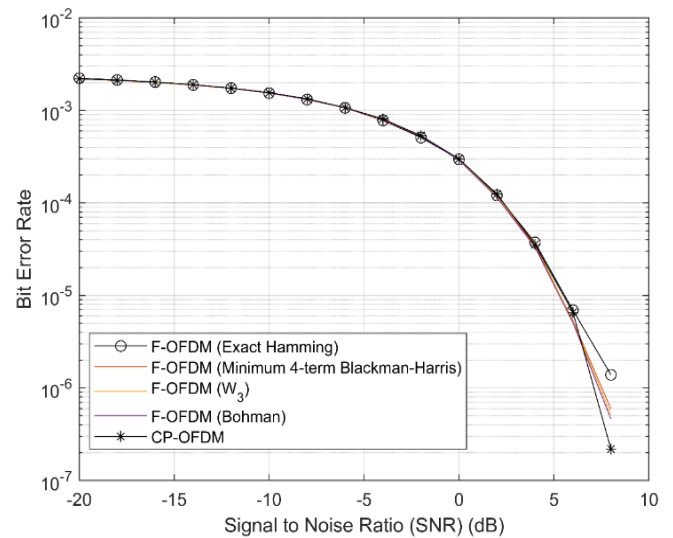


**Figure 7.** QPSK BER comparison between the suggested CP-OFDM, F-OFDM-based new window ( $W_3$ ), F-OFDM-based minimum 4-term Blackman-Harris window, F-OFDM-based Bohman window, and the Exact Hamming-based F-OFDM signals

Figure 8 shows the BER results of the 16QAM mapping for the CP-OFDM and the F-OFDM signals based on the new window ( $W_3$ ), F-OFDM-based minimum 4-term Blackman-Harris window, F-OFDM-based Bohman window, and the Exact Hamming based F-OFDM signals. However, it is shown that all the signals almost have the same value,  $2.55 \times 10^{-5}$ . That is, the suggested F-OFDM-based  $W_3$ -window did not degrade in terms of BER when compared with the benchmark signal

(CP-OFDM).

Simulation results, shown in Figures 7 and 8, indicate that the proposed window functions significantly reduce the BER and improve PSD compared to traditional CP-OFDM. The trade-offs between BER and PSD are managed effectively, demonstrating the flexibility and performance advantages of the combined window.

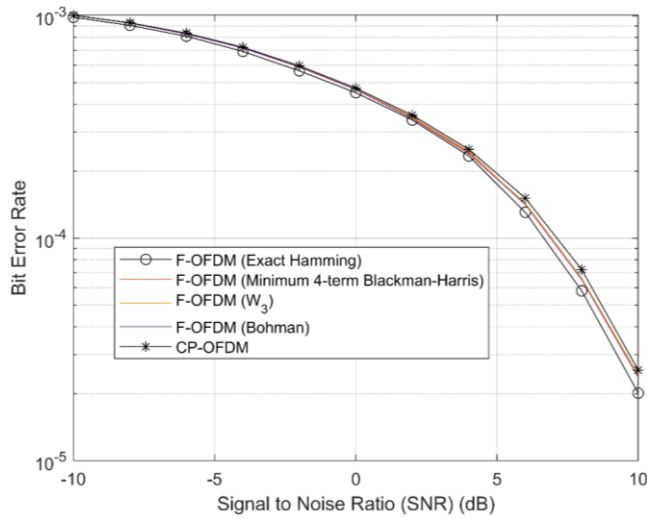


**Figure 8.** 16QAM BER comparison between the suggested CP-OFDM, F-OFDM-based new window ( $W_3$ ), F-OFDM-based minimum 4-term Blackman-Harris window, F-OFDM-based Bohman window, and the Exact Hamming-based F-OFDM signals

Furthermore, the other windows-based F-OFDM did not degrade with respect to the CP-OFDM signal in terms of BER, but in terms of PSD, F-OFDM-based  $W_3$ -window has an improved performance. The same attitude can be seen in Figure 9 for the 64QAM-based CP-OFDM and F-OFDM signals.

Last but not least, Figure 10 shows the BER comparison of the CP-OFDM and the F-OFDM signals based on the new window ( $W_3$ ), minimum 4-term Blackman-Harris window, Bohman window, and the Exact Hamming window. Nevertheless, there is no difference in the BER performance with respect to previous mappings, QPSK, 16QAM, and 64QAM, where all the signals perform similarly to each other, where the best BER was  $1.98 \times 10^{-4}$ .

To provide a more comprehensive evaluation, we summarize the trade-offs between spectral efficiency, complexity, and latency in Table 2.

**Table 2.** Summary of performance trade-offs between CP-OFDM and F-OFDM

Metric	CP-OFDM	F-OFDM	Improvement/Trade-off
Spectral efficiency	Moderate	High	20-25% improvement in spectral efficiency
Computational complexity	$O(N \log N)$	$O(N \log N) + O(NL)$	Increased complexity due to filtering
Latency	Low	Moderate	Additional latency proportional to $L$

In conclusion, the suggested F-OFDM-based  $W_3$ -window has improved the OBE performance without degrading the BER of the system. Even when the constellation mapping increased from QPSK to 256QAM, in other words, there is no matter when the number of bits of each subcarrier increased from 2 bits to 8 bits. Moreover, the proposed F-OFDM system offers significant improvements in spectral efficiency and

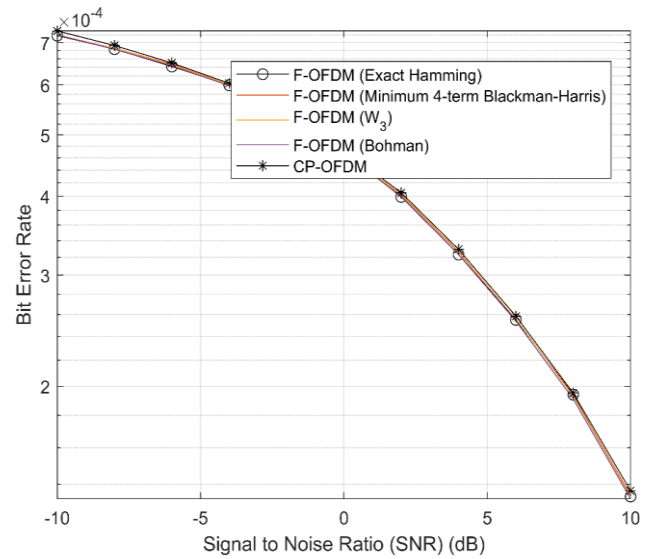


**Figure 9.** 64QAM BER comparison between the suggested CP-OFDM, F-OFDM-based new window ( $W_3$ ), F-OFDM-based minimum 4-term Blackman-Harris window, F-OFDM-based Bohman window, and the Exact Hamming-based F-OFDM signals

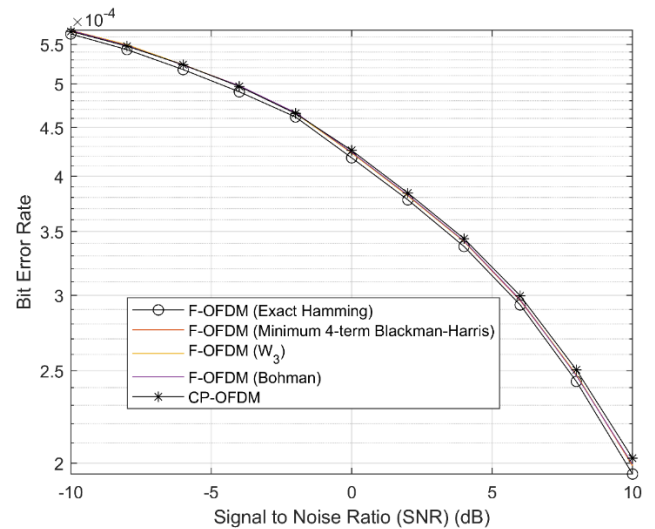


**Figure 10.** 256QAM BER comparison between the suggested CP-OFDM, F-OFDM-based new window ( $W_3$ ), F-OFDM-based minimum 4-term Blackman-Harris window, F-OFDM-based Bohman window, and the Exact Hamming-based F-OFDM signals

interference mitigation, making it suitable for next-generation wireless networks. However, these benefits come with trade-offs related to computational complexity, latency, and system flexibility. By carefully considering these trade-offs and employing optimization techniques, adaptive filtering, and hardware acceleration, the F-OFDM system can be tailored to meet the specific requirements of various applications, from

high-speed mobile communications to latency-sensitive IoT networks. Future research should focus on refining these trade-offs, exploring advanced interference management techniques, and optimizing the system for real-time performance.

The proposed window functions, Blackman-Harris and Bohman, improve the signal-to-noise ratio (SNR) by effectively reducing the power of side lobes and minimizing in-band noise. The Blackman-Harris window, with its low side lobe levels, ensures that less power is leaked outside the main lobe, resulting in a higher SNR. Mathematically, the SNR improvement can be represented as:

$$SNR_{improved} = 10 \log \left( \frac{P_{signal}}{P_{noise} + P_{side\ lobes}} \right) \quad (27)$$

where,  $P_{signal}$  is the power of the main lobe,  $P_{noise}$  is the in-band noise power, and  $P_{side\ lobes}$  is the power of the side lobes. By combining the Blackman-Harris and Bohman windows, we achieve an optimal balance, further enhancing SNR.

The proposed window functions also reduce inter-symbol and inter-carrier interference by smoothing transitions between symbols and minimizing spectral leakage. Theoretical backing for this reduction in interference is provided through the analysis of the window functions' impact on the frequency response:

$$I_{reduced} = \sum_{k \neq 0} |H(f - kf_s)|^2 \quad (28)$$

where,  $I_{reduced}$  represents the reduced interference,  $H(f)$  is the frequency response of the windowed signal, and  $kf_s$  denotes the subcarrier spacing. The combined window function minimizes  $|H(f - kf_s)|^2$ , leading to lower interference levels.

The proposed window functions improve spectral efficiency due to their ability to suppress side lobes while maintaining a narrow main lobe. This balance ensures that more subcarriers can be packed into the available spectrum without causing excessive interference. The spectral efficiency  $\eta$ , can be expressed as:

$$\eta = \frac{BER}{B} \quad (29)$$

where,  $BER$  is the bit rate and  $B$  is the bandwidth, the proposed window functions allow for a higher  $BE$  by reducing interference and noise, thereby improving  $\eta$ .

The theoretical analyses presented provide a deeper understanding of why the proposed method performs better. By reducing side lobe levels, the combined window function enhances SNR and spectral efficiency, leading to lower BER and improved PSD. These improvements are crucial for modern communication systems, particularly in scenarios where high spectral efficiency and low interference are required. The proposed method shows significant advantages over traditional CP-OFDM techniques, making it a valuable contribution to the field of signal processing.

## 8. CONCLUSIONS

Various concluding remarks are drawn in this work; these

remarks are as follows. The suggested window,  $W_3$ , was employed in the F-OFDM signal generation in order to reduce the out-of-band emission. However, it is concluded that the proposed window achieved its goal without degrading the performance of the power spectral density. The suggested window did not degrade the bit error rate performance. This innovative approach contributes to the novelty of our work, providing a significant improvement over existing window functions in the context of F-OFDM. Moreover, the constellation mapping was not an objection to using the suggested window, where the constellation mappings that are implemented to generate the CP-OFDM and the F-OFDM signals are QPSK, 16QAM, 64QAM, and 256QAM, in other words, 2-bits, 4-bits, 6-bits, and 8-bits, respectively, for each subcarrier. The key findings are:

**Enhanced spectral efficiency:** The application of F-OFDM significantly reduces OOB emissions compared to traditional OFDM, thus enhancing spectral efficiency.

**Improved interference mitigation:** By using a hybrid window function that combines the Blackman-Harris and Bohman windows, we achieved a balance between main lobe width and sidelobe suppression, which helps minimize interference from adjacent frequency bands.

**Flexible numerology multiplexing:** The F-OFDM system effectively supports multiple numerologies, making it suitable for various 5G services such as enhanced Mobile Broadband (eMBB), Ultra-Reliable Low-Latency Communications (URLLC), and massive Machine-Type Communications (mMTC).

Despite the promising results, the proposed system has some limitations:

**Computational complexity:** The filtering process, especially with subband filtering, adds computational complexity, which could be a challenge for real-time applications.

**Filter design:** The choice of filter parameters requires careful consideration to balance between performance and complexity. Suboptimal filter design can degrade system performance.

Finally, the future research directions are:

**Optimization of filter parameters:** Future work could focus on developing adaptive algorithms for optimal filter parameter selection to further enhance system performance and reduce computational complexity.

**Hardware implementation:** Implementing the F-OFDM system on hardware platforms such as Field-Programmable Gate Arrays (FPGAs) or Application-Specific Integrated Circuits (ASICs) to evaluate its real-time performance and feasibility.

## ACKNOWLEDGMENTS

The authors would like to acknowledge the support of Prince Sultan University for paying the Article Processing Charges (APC) of this publication. Special acknowledgement to Automated Systems and Soft Computing Lab (ASSCL), Prince Sultan University, Riyadh, Saudi Arabia.

## REFERENCES

- [1] Andrews, J.G., Buzzi, S., Choi, W., Hanly, S.V., Lozano, A., Soong, A.C., Zhang, J.C. (2014). What will 5G be?

- IEEE Journal on Selected Areas in Communications, 32(6): 1065-1082. <https://doi.org/10.1109/JSAC.2014.2328098>
- [2] ETSI TR 138900. (2017). Study on channel model for frequency spectrum above 6 GHz. [https://www.etsi.org/deliver/etsi\\_tr/138900\\_138999/138900/14.02.00\\_60/tr\\_138900v140200p.pdf](https://www.etsi.org/deliver/etsi_tr/138900_138999/138900/14.02.00_60/tr_138900v140200p.pdf).
- [3] ETSI TR 138913. (2017). Study on scenarios and requirements for next generation access technology. [https://www.etsi.org/deliver/etsi\\_tr/138900\\_138999/138913/14.02.00\\_60/tr\\_138913v140200p.pdf](https://www.etsi.org/deliver/etsi_tr/138900_138999/138913/14.02.00_60/tr_138913v140200p.pdf).
- [4] Yuan, Y., Wang, X. (2020). 5G new radio: Physical layer overview. *ZTE Communications*, 15(S1): 3-10. <https://doi.org/10.3969/j.issn.1673-5188.2017.S1.001>
- [5] Schaich, F., Wild, T., Chen, Y. (2014). Waveform contenders for 5G - Suitability for short packet and low latency transmissions. In 2014 IEEE 79th Vehicular Technology Conference (VTC Spring), Seoul, Korea (South), pp. 1-5. <https://doi.org/10.1109/VTCSpring.2014.7023145>
- [6] Banelli, P., Buzzi, S., Colavolpe, G., Modenini, A., Rusek, F., Ugolini, A. (2014). Modulation formats and waveforms for 5G networks: Who will be the heir of OFDM? An overview of alternative modulation schemes for improved spectral efficiency. *IEEE Signal Processing Magazine*, 31(6): 80-93. <https://doi.org/10.1109/MSP.2014.2337391>
- [7] Bellanger, M., Le Ruyet, D., Roviras, D., et al. (2010). FBMC physical layer: A primer. *Phydyas*, 25(4): 7-10.
- [8] Hammoodi, A., Audah, L., Taher, M.A. (2019). Green coexistence for 5G waveform candidates: A review. *IEEE Access*, 7: 10103-10126. <https://doi.org/10.1109/ACCESS.2019.2891312>
- [9] Bedoui, A., Et-tolba, M. (2017). A comparative analysis of filter bank multicarrier (FBMC) as 5G multiplexing technique. In 2017 International Conference on Wireless Networks and Mobile Communications (WINCOM), Rabat, Morocco, pp. 1-7. <https://doi.org/10.1109/WINCOM.2017.8238200>
- [10] Michailow, N., Matthé, M., Gaspar, I.S., et al. (2014). Generalized frequency division multiplexing for 5th generation cellular networks. *IEEE Transactions on Communications*, 62(9): 3045-3061. <https://doi.org/10.1109/TCOMM.2014.2345566>
- [11] Tang, N., He, S., Xue, C., Huang, Y., Yang, L. (2017). IQ imbalance compensation for generalized frequency division multiplexing systems. *IEEE Wireless Communications Letters*, 6(4): 422-425. <https://doi.org/10.1109/LWC.2017.2699961>
- [12] Wang, X., Wild, T., Schaich, F., Dos Santos, A.F. (2014). Universal filtered multi-carrier with leakage-based filter optimization. In European Wireless 2014; 20th European Wireless Conference, Barcelona, Spain, pp. 1-5.
- [13] Wild, T., Schaich, F., Chen, Y. (2014). 5G air interface design based on Universal Filtered (UF-)OFDM. In 2014 19th International Conference on Digital Signal Processing, Hong Kong, China, pp. 699-704. <https://doi.org/10.1109/ICDSP.2014.6900754>
- [14] Lu, S., Qu, D., He, Y. (2012). Sliding window tone reservation technique for the peak-to-average power ratio reduction of FBMC-OQAM signals. *IEEE Wireless Communications Letters*, 1(4): 268-271. <https://doi.org/10.1109/WCL.2012.062512.120360>
- [15] Cheng, X., He, Y., Ge, B., He, C. (2016). A filtered OFDM using FIR filter based on window function method. In 2016 IEEE 83rd Vehicular Technology Conference (VTC Spring), Nanjing, China, pp. 1-5. <https://doi.org/10.1109/VTCSpring.2016.7504065>
- [16] Li, J., Bala, E., Yang, R. (2014). Resource block filtered-OFDM for future spectrally agile and power efficient systems. *Physical Communication*, 11: 36-55. <https://doi.org/10.1016/j.phycom.2013.10.003>
- [17] Zhang, X., Jia, M., Chen, L., Ma, J., Qiu, J. (2015). Filtered-OFDM - Enabler for flexible waveform in the 5th generation cellular networks. In 2015 IEEE Global Communications Conference (GLOBECOM), San Diego, CA, USA, pp. 1-6. <https://doi.org/10.1109/GLOCOM.2015.7417854>
- [18] Abdoli, J., Jia, M., Ma, J. (2015). Filtered OFDM: A new waveform for future wireless systems. In 2015 IEEE 16th International Workshop on Signal Processing Advances in Wireless Communications (SPAWC), Stockholm, Sweden, pp. 66-70. <https://doi.org/10.1109/SPAWC.2015.7227001>
- [19] An, C., Kim, B., Ryu, H.G. (2017). WF-OFDM (windowing and filtering OFDM) system for the 5G new radio waveform. In 2017 IEEE XXIV International Conference on Electronics, Electrical Engineering and Computing (INTERCON), Cusco, Peru, pp. 1-4. <https://doi.org/10.1109/INTERCON.2017.8079635>
- [20] Wang, J., Jin, A., Shi, D., et al. (2017). Spectral efficiency improvement with 5G technologies: Results from field tests. *IEEE Journal on Selected Areas in Communications*, 35(8): 1867-1875. <https://doi.org/10.1109/JSAC.2017.2713498>
- [21] Li, J., Kearney, K., Bala, E., Yang, R. (2013). A resource block based filtered OFDM scheme and performance comparison. In ICT 2013, Casablanca, Morocco, pp. 1-5. <https://doi.org/10.1109/ICTEL.2013.6632084>
- [22] Bazzi, J., Weitkemper, P., Kusume, K., Benjebbour, A., Kishiyama, Y. (2015). Design and performance tradeoffs of alternative multicarrier waveforms for 5G. In 2015 IEEE Globecom Workshops (GC Wkshps), San Diego, CA, USA, pp. 1-6. <https://doi.org/10.1109/GLOCOMW.2015.7414010>
- [23] Wu, D., Zhang, X., Qiu, J., Gu, L., Saito, Y., Benjebbour, A., Kishiyama, Y. (2016). A field trial of f-OFDM toward 5G. In 2016 IEEE Globecom Workshops (GC Wkshps), Washington, DC, USA, pp. 1-6. <https://doi.org/10.1109/GLOCOMW.2016.7848810>
- [24] Hu, K.C., Armada, A.G. (2016). SINR analysis of OFDM and f-OFDM for machine type communications. In 2016 IEEE 27th Annual International Symposium on Personal, Indoor, and Mobile Radio Communications (PIMRC), Valencia, Spain, pp. 1-6. <https://doi.org/10.1109/PIMRC.2016.7794702>
- [25] Augustine, Z., Bello, H., Tekanyi, A.M.S., Yaro, A.S., Abdulkareem, H.A., Abdu-Aguye, U.F. (2024). Generation of 5G frequency one model based on orthogonal multiple access technique of filtered-orthogonal frequency division multiplexing scheme for advanced interference evaluation. <http://doi.org/10.2139/ssrn.4734816>
- [26] Ramineni, P., Yellagalla, M., Rajpet, B. (2024). Evaluation of modulation techniques for 5G wireless communication: A performance comparison of OFDM, F-OFDM, UPMC and FBMC in terms of PSD, BER and SNR Metrics. *Journal of Engineering Research and*

- Reports, 26(7): 285-299. <https://doi.org/10.9734/jerr/2024/v26i71209>
- [27] El Ghzaoui, M. (2024). CPM modulation implementation using blind equalizer and non-coherent demodulation for 5G and beyond. *International Journal of System Assurance Engineering and Management*, 15: 2097-2104. <https://doi.org/10.1007/s13198-023-02211-9>
- [28] ETSI TS 138211. (2018). 5G; NR; Physical channels and modulation. [https://www.etsi.org/deliver/etsi\\_ts/138200\\_138299/138211/15.02.00\\_60/ts\\_138211v150200p.pdf](https://www.etsi.org/deliver/etsi_ts/138200_138299/138211/15.02.00_60/ts_138211v150200p.pdf).
- [29] ETSI TR 138901. (2020). 5G: Study on channel model for frequencies from 0.5 to 100 GHz. [https://www.etsi.org/deliver/etsi\\_tr/138900\\_138999/138901/16.01.00\\_60/tr\\_138901v160100p.pdf](https://www.etsi.org/deliver/etsi_tr/138900_138999/138901/16.01.00_60/tr_138901v160100p.pdf).
- [30] Dahlman, E., Mildh, G., Parkvall, S., Peisa, J., Sachs, J., Selén, Y., Sköld, J. (2014). 5G wireless access: requirements and realization. *IEEE Communications Magazine*, 52(12): 42-47. <https://doi.org/10.1109/MCOM.2014.6979985>
- [31] Vook, F.W., Ghosh, A., Diarte, E., Murphy, M. (2018). 5G new radio: Overview and performance. In 2018 52nd Asilomar Conference on Signals, Systems, and Computers, Pacific Grove, CA, USA, pp. 1247-1251. <https://doi.org/10.1109/ACSSC.2018.8645228>
- [32] Bingham, J.A.C. (1990). Multicarrier modulation for data transmission: An idea whose time has come. *IEEE Communications Magazine*, 28(5): 5-14. <https://doi.org/10.1109/35.54342>
- [33] Ku, G., Walsh, J.M. (2015). Resource allocation and link adaptation in LTE and LTE Advanced: A tutorial. *IEEE Communications Surveys & Tutorials*, 17(3): 1605-1633. <https://doi.org/10.1109/COMST.2014.2383691>
- [34] Fulop, S.A., Fitz, K. (2006). Algorithms for computing the time-corrected instantaneous frequency (reassigned) spectrogram, with applications. *The Journal of the Acoustical Society of America*, 119(1): 360-371. <https://doi.org/10.1121/1.2133000>
- [35] Harris, F.J. (1978). On the use of windows for harmonic analysis with the discrete Fourier transform. *Proceedings of the IEEE*, 66(1): 51-83. <https://doi.org/10.1109/PROC.1978.10837>
- [36] Taher, M.A., Radhi, H.S., Jameil, A.K. (2021). Enhanced F-OFDM candidate for 5G applications. *Journal of Ambient Intelligence and Humanized Computing*, 12(1): 635-652. <https://doi.org/10.1007/s12652-020-02046-3>
- [37] Yousaf, K., Mehmood, Z., Saba, T., Rehman, A., Rashid, M., Altaf, M., Shuguang, Z. (2018). A novel technique for speech recognition and visualization based mobile application to support two-way communication between deaf-mute and normal peoples. *Wireless Communications and Mobile Computing*, 2018(1): 1013234. <https://doi.org/10.1155/2018/1013234>
- [38] Rehman, A., Saba, T., Haseeb, K., Singh, R., Jeon, G. (2022). Smart health analysis system using regression analysis with iterative hashing for IoT communication networks. *Computers and Electrical Engineering*, 104: 108456. <https://doi.org/10.1016/j.compeleceng.2022.108456>
- [39] Jadooki, S., Mohamad, D., Saba, T., Almazayad, A.S., Rehman, A. (2017). Fused features mining for depth-based hand gesture recognition to classify blind human communication. *Neural Computing and Applications*, 28: 3285-3294. <https://doi.org/10.1007/s00521-016-2244-5>
- [40] Taha, A., Alsaqour, R., Uddin, M., Abdelhaq, M., Saba, T. (2017). Energy efficient multipath routing protocol for mobile ad-hoc network using the fitness function. *IEEE Access*, 5: 10369-10381. <https://doi.org/10.1109/ACCESS.2017.2707537>
- [41] Anter, A.M., Hassanien, A.E., ElSoud, M.A., Azar, A.T. (2015). Automatic liver parenchyma segmentation system from abdominal CT scans using hybrid techniques. *International Journal of Biomedical Engineering and Technology*, 17(2): 148-167. <https://doi.org/10.1504/IJBET.2015.068052>
- [42] Atteia, G., El-Kenawy, E.S.M., Samee, N.A., et al. (2023). Adaptive dynamic dipper throated optimization for feature selection in medical data. *Computers, Materials & Continua*, 75(1): 1883-1900. <http://doi.org/10.32604/cmc.2023.031723>
- [43] Aziz, A.S.A., Azar, A.T., Salama, M.A., Hassanien, A.E., Hanafy, S.E.O. (2013). Genetic algorithm with different feature selection techniques for anomaly detectors generation. In 2013 Federated Conference on Computer Science and Information Systems, Krakow, Poland, pp. 769-774.
- [44] Elshazly, H.I., Elkorany, A.M., Hassanien, A.E., Azar, A.T. (2013). Ensemble classifiers for biomedical data: Performance evaluation. In 2013 8th International Conference on Computer Engineering & Systems (ICCES), Cairo, Egypt, pp. 184-189. <https://doi.org/10.1109/ICCES.2013.6707198>